



ORIGINAL ARTICLE

L-cysteine-regulated in situ formation of Prussian blue/Turnbull's blue nanoparticles as the colorimetric probe for the detection of copper ion



Hang-Yu Zhou^a, Hao Zhang^{b,*}, Li-Jing Peng^a, Wei-Yi Zhang^a, Tao Tian^a,
Feng-Qing Yang^{a,*}

^a School of Chemistry and Chemical Engineering, Chongqing University, Chongqing 401331, China

^b Chongqing Key Laboratory of High Active Traditional Chinese Drug Delivery System, Chongqing Medical and Pharmaceutical College, Chongqing 401331, China

Received 27 March 2022; accepted 22 May 2022

Available online 26 May 2022

KEYWORDS

Copper ion;
L-cysteine;
Prussian blue/Turnbull's
blue nanoparticles;
Aggregation;
Colorimetric detection

Abstract A fast, simple, sensitive, and selective colorimetric method for the detection of Cu^{2+} was developed using Prussian blue/Turnbull's blue nanoparticles (PBNPs/TBNPs) as the probe. The colorimetric sensor is based on the following principle. Cu^{2+} can induce the aggregation of L-cysteine (L-cys) modified-PBNPs/TBNPs (L-cys-PBNPs/TBNPs), resulting in an obvious red shift of its maximum absorption peak. Thus, the concentration of Cu^{2+} can be determined based on the peak shift in the UV-Vis spectra. The optimal pH, concentration of L-cys, reaction temperature between L-cys-PBNPs/TBNPs and Cu^{2+} , the formation time of L-cys-PBNPs/TBNPs, and the reaction time between L-cys-PBNPs/TBNPs and Cu^{2+} of the method were determined to be pH 4.5, 2.0 mM, 20 °C, 5.0 min, and 2.0 min, respectively. A good linearity for the colorimetric determination of Cu^{2+} at the range of 0.25–2.5 μM ($R^2 = 0.986$) was obtained, with a limit of detection (LOD) of 0.12 μM . Moreover, the negligible response of other metal ions demonstrates good selectivity and specificity of the sensor. In addition, the method was employed in the detection of Cu^{2+} in lake water samples, and the spiked recoveries are in the range of 96.7–106.6% with a relative standard deviation less than 7.4%. Therefore, the colorimetric method is applicable for Cu^{2+} detection in real water samples of high sensitivity and selectivity.

© 2022 The Author(s). Published by Elsevier B.V. on behalf of King Saud University. This is an open access article under the CC BY-NC-ND license (<http://creativecommons.org/licenses/by-nc-nd/4.0/>).

* Corresponding authors at: School of Chemistry and Chemical Engineering, Chongqing University, Chongqing 401331, China. (F.-Q. Yang). Chongqing Key Laboratory of High Active Traditional Chinese Drug Delivery System, Chongqing Medical and Pharmaceutical College, Chongqing 401331, China (H. Zhang).

E-mail addresses: zhanghao199392@163.com (H. Zhang), fengqingyang@cqu.edu.cn (F.-Q. Yang).

Peer review under responsibility of King Saud University.



1. Introduction

As one of the essential micronutrients for organisms, copper (Cu) plays important roles in numerous biological processes such as serving as a redox-active catalytic centre in enzymes cycling between Cu^+ and Cu^{2+} (Falcone et al., 2021). However, elevated concentration of Cu^{2+} may lead to DNA damage (Trumbore et al., 2001), liver damage to children (Zietza et al., 2003), and low-density lipoprotein oxidation (Witting et al., 1995). In addition, the disorders of copper homeostasis will cause serious neurodegenerative diseases such as Menkes disease, Wilson disease, and Alzheimer's disease (Kim et al., 2008). On the other hand, the high level of Cu^{2+} can also cause serious environmental issues because excessive Cu^{2+} will affect the survival of fish, shellfish, and bacteria, and may further damage the self-purification ability of natural water systems (Aksuner et al., 2009). Therefore, the US Environmental Protection Agency (EPA) has listed Cu^{2+} as a major pollutant and the maximum contaminant level (MCL) of Cu^{2+} in drinking water is set at $20.0 \mu\text{M}$ (Gao et al., 2017). Herein, it is of significant importance to develop sensitive and selective methods for Cu^{2+} detection.

Up to now, various analytical methods have been developed for Cu^{2+} detection, including inductively coupled plasma mass spectrometry (ICP-MS), atomic absorption spectroscopy (AAS), electrochemical techniques, and fluorescence methods (Yin et al., 2015). Although ICP-MS and AAS can achieve highly sensitive detection for Cu^{2+} , the demand for large and expensive instruments, and professional staff hampers their widely applications (Yin et al., 2015). The synthesis of fluorescent probes usually requires toxic and insoluble chemical reagents, time-consuming preparation steps, and complicated purification processes, which restricts its application (Ma et al., 2011a, 2011b). The electrochemical techniques for Cu^{2+} detection has the drawback that the detection signal is unstable (Ramdass et al., 2017). On the other hand, colorimetric strategies have received extensive attention for it is simple detection by naked eyes and UV-Vis spectroscopy (Yin et al., 2015). Recently, a series of nanomaterials-based colorimetric sensors, such as silver nanoparticles (Ma et al., 2011a, 2011b), gold nanoparticles (AuNPs) (Li and Li 2009), and gold nanorods (Liu et al., 2011), have been widely used in the detection of various molecules and ions. However, silver nanoparticles are unstable (Liu et al., 2013), and the synthesis of gold nanorods is complex and costly, which may limit their further applications.

As an ancient dye, Prussian blue (PB) was firstly discovered by a Berlin artist Diesbach in 1704 (Griffith 1962), and its electrochemical properties were reported until 1978 (Neff 1978). Since then, more and more studies about the electrochemical (Itaya et al., 1982) and electrochromic (Wang et al., 2014, Yeon et al., 2022) properties of PB have been reported. PB is a prototype of mixed-valence transition metal hexacyanoferrates (Fu et al., 2016), and its face-centered cubic unit cell is composed of ferric, ferrous, and cyanide ions (Qin et al., 2018). PB has been widely used as an indicator in electrochemical sensors (Wei et al., 2021). It is also widely applied in the biomedicine and biosensors for its favorable biocompatibility and unique property (Zhang et al., 2016). In addition, PB is a drug approved by the Food and Drug Administration (FDA) for the treatment of thallium poisoning (Jing et al., 2014). What's more, PB has been proven to have peroxidase-like activity that can catalyze the reduction of hydrogen peroxide. Kavitha et al. utilized the peroxidase-like activity of PB to realize the detection of Cu^{2+} and cysteine (Kavitha et al., 2021). In reality, PB can be also served as optical probes because it has an intense absorption band near 700 nm due to an electron transfer from ground state $\text{Fe}_A(\text{III})\text{Fe}_B(\text{II})$ to an excited state $\text{Fe}_A(\text{II})\text{Fe}_B(\text{III})$ (Nóbrega and Lopes 1996, Zargar and Hatamie 2014, Zaręba et al., 2016). Zhang et al. developed a photothermometric biosensor to detect ascorbate oxidase based on redox reaction-controlled nanoprobe conversion from Prussian blue to Prussian white (Zhang et al., 2021).

Huang et al. proposed a method to detect silver ions based on the absorbance alteration or color change of Prussian blue nanoparticles (PBNPs) (Huang et al., 2017).

In this study, L-cysteine (L-cys) modified-PBNPs/Turnbull's blue (TBNPs) (L-cys-PBNPs/TBNPs) was prepared and used as the probe to realize the sensitive and selective detection of Cu^{2+} for the first time. With the addition of Cu^{2+} , an obvious red shift of the maximum absorption peak of L-cys-PBNPs/TBNPs can be observed. As compared to other published methods for Cu^{2+} detection, the proposed L-cys-PBNPs/TBNPs-based colorimetric sensor is expected to have the following advantages. (1) A relatively low cost; (2) A simple preparation process of L-cys-PBNPs/TBNPs; (3) The high selectivity for Cu^{2+} detection due to the special affinity between Cu^{2+} and L-cys modified on PBNPs/TBNPs; (4) Rapid detection of Cu^{2+} . After the experimental conditions being systematically optimized, the developed colorimetric method was utilized in the detection of Cu^{2+} in real water samples.

2. Materials and methods

2.1. Chemicals and materials

Copper (II) sulfate pentahydrate ($\text{CuSO}_4 \cdot 5\text{H}_2\text{O}$) and acetic acid (HAc) were purchased from Chongqing Chuandong Chemical (group) Co., Ltd. (Chongqing, China). Sodium acetate trihydrate ($\text{NaAc} \cdot 3\text{H}_2\text{O}$) and cobalt (II) chloride hexahydrate ($\text{CoCl}_2 \cdot 6\text{H}_2\text{O}$) were purchased from Shanghai Titan Scientific Co., Ltd. (Shanghai, China). Lead nitrate ($\text{Pb}(\text{NO}_3)_2$), barium chloride dihydrate ($\text{BaCl}_2 \cdot 2\text{H}_2\text{O}$), zinc sulfate heptahydrate ($\text{ZnSO}_4 \cdot 7\text{H}_2\text{O}$), aluminum nitrate nonahydrate ($\text{Al}(\text{NO}_3)_3 \cdot 9\text{H}_2\text{O}$), sodium chloride (NaCl), potassium chloride (KCl), silver nitrate (AgNO_3), and magnesium sulfate heptahydrate ($\text{MgSO}_4 \cdot 7\text{H}_2\text{O}$) were obtained from Chengdu Chron Chemicals Co., Ltd. (Chengdu, China). L-cysteine and manganese chloride ($\text{MnCl}_4 \cdot 4\text{H}_2\text{O}$) were obtained from Shanghai Aladdin Biochemical Technology Co., Ltd. (Shanghai, China). Calcium chloride anhydrous (CaCl_2) was purchased from Tianjin Damao Chemical Reagent Factory (Tianjin, China). Iron (III) chloride (FeCl_3) and potassium hexacyanoferrate (III) ($\text{K}_3[\text{Fe}(\text{CN})_6]$) were obtained from Shanghai Adamas Reagent Co., Ltd. (Shanghai, China). Potassium hexacyanoferrate (K₄[Fe(CN)₆]) was purchased from Shanghai Macklin Biochemical Co., Ltd. (Shanghai, China).

2.2. Instruments

Fourier transform infrared (FT-IR) spectra ($4000\text{--}400 \text{ cm}^{-1}$) were collected on a Nicolet 550 II (Thermo Scientific Inc., USA) FT-IR spectrometer with KBr media. X-ray diffraction (XRD) patterns of the prepared materials were obtained using X'pert Powder diffractometer (Malvern Panalytical Ltd., the Netherlands) with secondary beam graphite monochromated Cu K α radiation. The pH of solutions was measured using a FE 28 pH meter (Mettler-Toledo Instruments, Shanghai). The temperature was controlled by a SHZ-82 vapour-bathing constant temperature vibrator (Jintan Chengxi Zhen-gong Experimental Instrument Factory, Jiangsu, China). Transmission electron microscopy (TEM) images were recorded using a Talos F200S (Thermo Fisher Scientific Co., Ltd. Czech Republic). UV-Vis analysis was performed on a UV-8000S spectrophotometer (Shanghai Metash Instruments

Co., Ltd., Shanghai, China). All the solutions were prepared in deionized water.

2.3. Preparation of buffer and sample solutions

The L-cys (8.0 mM), FeCl₃ (4.0 mM), FeCl₂ (4.0 mM), K₃[Fe(CN)₆] (50.0 mM), and K₄[Fe(CN)₆] (50.0 mM) solutions were all prepared by dissolving them in NaAc-HAc buffer (0.2 M, pH 4.5), respectively. Different concentrations of Cu²⁺ solutions (0.25, 0.5, 1.25, 2.0, and 2.5 μM) were prepared by dissolving CuSO₄·5H₂O in NaAc-HAc buffer (0.2 M, pH 4.5).

2.4. Preparation of L-cys-PBNPs/TBNPs

L-cys-PBNPs/TBNPs were prepared by adding 50.0 μL of 8.0 mM of L-cys, 1.0 μL of 50.0 mM of K₃[Fe(CN)₆], and 50.0 μL of 4.0 mM of FeCl₃ into 99.0 μL of NaAc-HAc buffer (0.2 M, pH 4.5) and reacted for 5.0 min at 20 °C. The prepared L-cys-PBNPs/TBNPs can be used for Cu²⁺ detection immediately.

2.5. Colorimetric determination of Cu²⁺

In a typical procedure, 100.0 μL of Cu²⁺ solution and 100.0 μL of deionized water were added into 200.0 μL of the prepared L-cys-PBNPs/TBNPs solution and reacted for 2.0 min at 20 °C. There is an obvious red shift of the maximum absorption peak of L-cys-PBNPs/TBNPs in this process and the blue color of the solution turns to shallow blue. Then, the UV-Vis spectra in the range of 450–950 nm of the samples were recorded, and the red shift Δλ (Δλ = λ - λ₀, where λ₀ and λ are the maximum absorption peak wavelength of L-cys-PBNPs/TBNPs in the absence and presence of Cu²⁺, respectively) was calculated. Finally, the calibration curve between Cu²⁺ concentration and Δλ was plotted for the determination of Cu²⁺.

2.6. Specificity for the Cu²⁺ detection

To evaluate the selectivity and specificity of the developed probe for Cu²⁺ detection, the following ions were analyzed

under optimal conditions: Na⁺, K⁺, Ag⁺, Pb²⁺, Ca²⁺, Mn²⁺, Co²⁺, Mg²⁺, Zn²⁺, Ba²⁺, Fe³⁺, and Al³⁺. The final concentrations of Cu²⁺ and other metal ions are 2.5 μM and 5.0 μM, respectively.

2.7. Detection of Cu²⁺ in real sample

The colorimetric sensor was applied in the detection of Cu²⁺ in real water samples, which were collected from Yun Lake and Jin Lake at Chongqing University. All the water samples were filtered through 0.22 μm membrane to remove particulate matters before analysis.

3. Results and discussion

3.1. Sensing principle

Fig. 1 depicts the principle of the proposed colorimetric sensor. L-cys can reduce K₃[Fe(CN)₆] and Fe³⁺ to K₄[Fe(CN)₆] and Fe²⁺, respectively. In the case of co-existence of K₃[Fe(CN)₆], K₄[Fe(CN)₆], Fe³⁺, and Fe²⁺, K₄[Fe(CN)₆] can couple with Fe³⁺ exclusively to generate Fe₄[Fe(CN)₆]₃ nanoparticles (PBNPs) (Qin et al., 2018). At the same time, K₃[Fe(CN)₆] can also combine with Fe²⁺ to produce Fe₃[Fe(CN)₆]₂ nanoparticles (TBNPs) (Reguera et al., 1999). As a result, the mixture appears a blue color. And during the formation of PBNPs and TBNPs, L-cys can combine with them probably through Fe-S bond to form L-cys-PBNPs/TBNPs. On the other hand, Cu²⁺ can bind to L-cys-PBNPs/TBNPs through coordination with acidic (–COOH) and basic (–NH₂) functional groups of L-cysteine (Liu et al., 2011). Based on this principle, the introduction of Cu²⁺ will contribute to the aggregation of L-cys-PBNPs/TBNPs, resulting in the red shift of its maximum absorption peak. Therefore, quantitatively determination of Cu²⁺ can be achieved according to the co-relationship between Cu²⁺ concentration and peak-shift value.

3.2. Characterizations of L-cys-PBNPs/TBNPs

The presence of functional groups on the materials were investigated using FT-IR spectroscopy (Fig. S1). In the FT-IR spec-

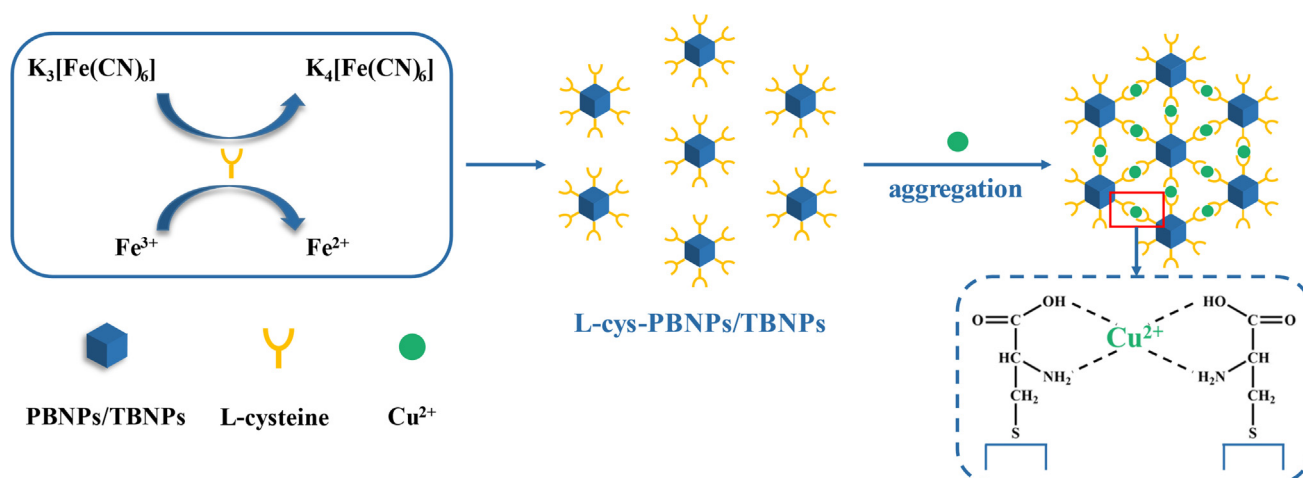


Fig. 1 Mechanism of Cu²⁺ detection using the L-cys-PBNPs/TBNPs as colorimetric probe.

trum of Fig. S1a, the peak at 2083 cm^{-1} is accredited to the $\text{C}\equiv\text{N}$ stretching vibration of PBNPs. And the absorption band at 495 cm^{-1} can be contributing to the formation of M-CN-M' structure (M = metal). Both the bands confirm the formation of PBNPs/TBNPs. In addition, the L-cys-PBNPs/TBNPs reacting with Cu^{2+} (Fig. S1b) also has a $\text{C}\equiv\text{N}$ stretching vibration peak at 2074 cm^{-1} and M-CN-M' structure peak at 498 cm^{-1} , suggesting that Cu^{2+} will not affect the chemical composition of L-cys-PBNPs/TBNPs.

The crystalline structure of L-cys-PBNPs/TBNPs was characterized through XRD. As shown in Fig. S2a, the diffractions of L-cys-PBNPs/TBNPs are corresponded to the (200), (220), (222), (400), (420), (422), (440), (531), and (620) phases of PB according to the standard card (JCPDS card no.73-0687). However, the crystalline structure of L-cys-PBNPs/TBNPs was slightly influenced after reacting with Cu^{2+} as observed in Fig. S2b.

The morphologies of L-cys-PBNPs/TBNPs were characterized by TEM. As shown in Fig. S3 and Fig. 2A, L-cys-PBNPs/TBNPs are granular nanoparticles with a size of about 25 nm. However, L-cys-PBNPs/TBNPs are connected into a branches' shape after the addition of Cu^{2+} (Fig. 2B), indicating that the introduction of Cu^{2+} promotes the large-scale aggregation of L-cys-PBNPs/TBNPs. In addition, the energy dispersive spectroscopy (EDS) elemental mapping images (Fig. S4) indicate the existence of elements C, Fe, N, O, and S, further proving the success in synthesis of L-cys-PBNPs/TBNPs. Furthermore, the existences of elements S and O prove that PBNPs/TBNPs are modified by L-cys. As shown in Fig. S5, the existences of element C, Fe, N, O, S, and Cu prove that the aggregation of L-cys-PBNPs/TBNPs is caused by the addition of Cu^{2+} .

3.3. Feasibility study

L-cys plays an important role in reducing $\text{K}_3[\text{Fe}(\text{CN})_6]$ to $\text{K}_4[\text{Fe}(\text{CN})_6]$ and Fe^{3+} to Fe^{2+} . As shown in Fig. 3a, without L-cys, there is no absorption band at 450–950 nm and no color change when only mixing FeCl_3 and $\text{K}_3[\text{Fe}(\text{CN})_6]$. Furthermore, as shown in Fig. 3b, the color of the mixture solution still keeps colorless and there is no absorption band after addition of Cu^{2+} , indicating that Cu^{2+} cannot reduce $\text{K}_3[\text{Fe}(\text{CN})_6]$ or Fe^{3+} . However, when mixing L-cys, FeCl_3 , and $\text{K}_3[\text{Fe}(\text{CN})_6]$, the solution shows a blue color and a new absorption peak can be observed at a wavelength of 717 nm (Fig. 3c). L-cys-PBNPs/TBNPs are formed as $\text{K}_3[\text{Fe}(\text{CN})_6]$ and Fe^{3+} being reduced to $\text{K}_4[\text{Fe}(\text{CN})_6]$ and Fe^{2+} by L-cys, respectively. After the addition of $5.0\text{ }\mu\text{M}$ of Cu^{2+} , the maximum absorption peak exhibits an obvious red shift from 717 nm to 747 nm of L-cys-PBNPs/TBNPs and its absorption is decreased as observed in Fig. 3d. The decrease of the absorption may be due to the high scattering caused by the aggregation of L-cys-PBNPs/TBNPs in the presence of Cu^{2+} . And another part of reason is that $\text{Fe}_3[\text{Fe}(\text{CN})_6]_2$ may be transformed into $\text{Cu}_3[\text{Fe}(\text{CN})_6]_2$ after addition of Cu^{2+} as the reducibility of Cu^{2+} is stronger than that of Fe^{2+} .

The control experiments were also performed to investigate the pivotal role of L-cys and the reasons for the decrease in absorption of L-cys-PBNPs/TBNPs. Firstly, $\text{K}_4[\text{Fe}(\text{CN})_6]$ was added to FeCl_3 solution to form PBNPs directly and the mixture solution turns to blue (Fig. S6A). A new absorption peak was observed at a wavelength of 697 nm. There is no sig-

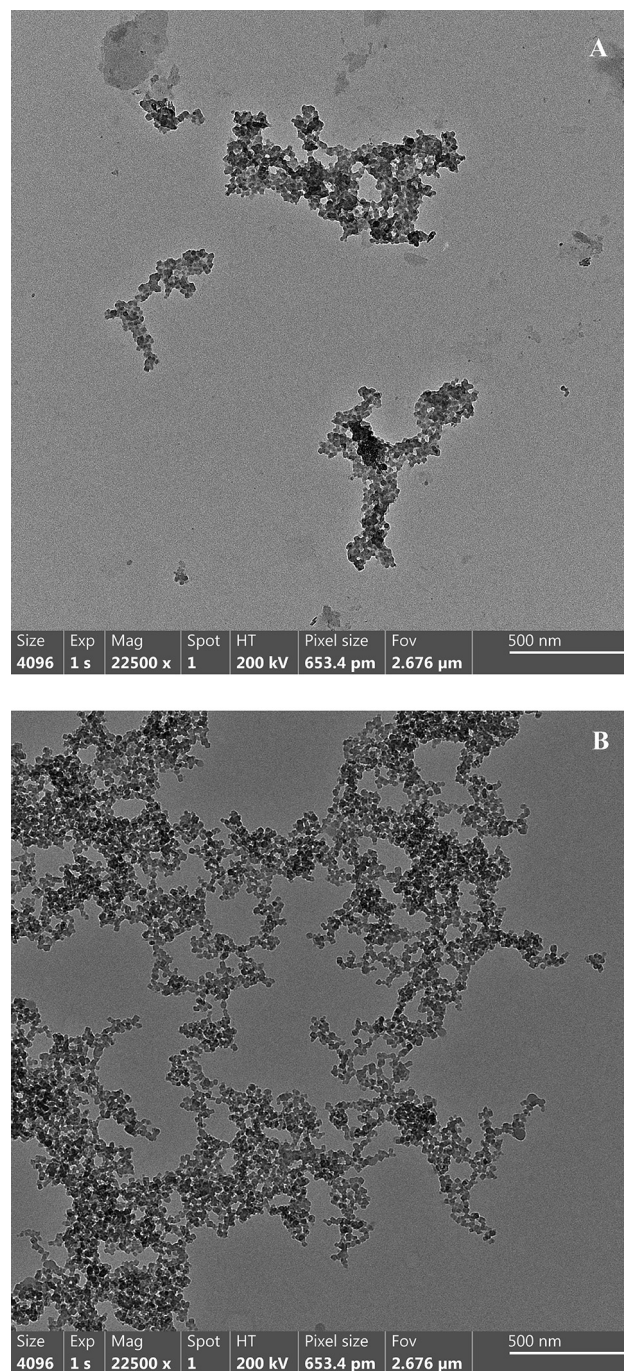


Fig. 2 TEM images of L-cys-PBNPs/TBNPs before (A) and after (B) the addition of Cu^{2+} (magnification times: 22500).

nificantly red shift or absorption decrease after introducing $5.0\text{ }\mu\text{M}$ or $100.0\text{ }\mu\text{M}$ of Cu^{2+} to the above-mentioned mixture, respectively. Then, $\text{K}_3[\text{Fe}(\text{CN})_6]$ was added to FeCl_2 solution to form TBNPs directly and the mixture also turns to blue. A new absorption peak is observed at a wavelength of 729 nm as shown in Fig. S6B. However, after adding $5.0\text{ }\mu\text{M}$ or $100.0\text{ }\mu\text{M}$ of Cu^{2+} to the mixture, the absorption is decreased as observed in Fig. S6B, indicating that $\text{Fe}_3[\text{Fe}(\text{CN})_6]_2$ may transform to $\text{Cu}_3[\text{Fe}(\text{CN})_6]_2$ in the presence of Cu^{2+} cause the reducibility of Cu^{2+} is stronger than that of Fe^{2+} . The absorption does not decrease significantly when

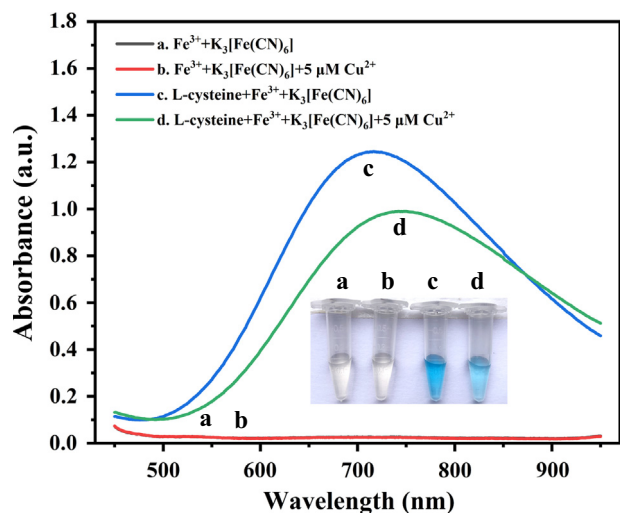


Fig. 3 UV-Vis spectra of the mixture solutions under different conditions. $\text{Fe}^{3+} + \text{K}_3[\text{Fe}(\text{CN})_6]$ (a), $\text{Fe}^{3+} + \text{K}_3[\text{Fe}(\text{CN})_6] + \text{Cu}^{2+}$ (b), L-cys + $\text{Fe}^{3+} + \text{K}_3[\text{Fe}(\text{CN})_6]$ (c), L-cys + $\text{Fe}^{3+} + \text{K}_3[\text{Fe}(\text{CN})_6] + \text{Cu}^{2+}$ (d). Inset is the corresponding photograph. The final concentrations of L-cys, FeCl_3 , $\text{K}_3[\text{Fe}(\text{CN})_6]$, and Cu^{2+} solutions are 2.0 mM, 1.0 mM, 0.25 mM, and 5.0 μM , respectively; the pH of NaAc-HAc buffer and reaction temperature between L-cys and Cu^{2+} are 4.5 and 30 $^\circ\text{C}$, respectively; both of the formation time of L-cys-PBNPs/TBNPs and reaction time between L-cys-PBNPs/TBNPs and Cu^{2+} are 5.0 min.

only adding 5.0 μM of Cu^{2+} , but decreases much after introducing 100.0 μM of Cu^{2+} , suggesting that the addition of Cu^{2+} can reduce the absorption of TBNPs. Then, L-cys was introduced after the formation of PBNPs and TBNPs, and reacted for 5.0 min, respectively. As shown in Fig. S6C and Fig. S6D, an obvious red shift of the maximum absorption peak of L-cys-PBNPs/TBNPs was observed after addition of Cu^{2+} , which may be because of the high affinity between L-cys and Cu^{2+} . The decrease in absorption may be due to two parts of reasons, the main reason is that the high scattering caused by the aggregation of L-cys-PBNPs/TBNPs in the presence of Cu^{2+} , another is that the addition of Cu^{2+} can reduce the absorption of TBNPs.

3.4. Optimization of the sensor for the detection of Cu^{2+}

The colorimetric response of L-cys-PBNPs/TBNPs towards Cu^{2+} depends on several key parameters. Therefore, the pH of NaAc-HAc buffer, concentration of L-cys, reaction temperature between L-cys-PBNPs/TBNPs and Cu^{2+} , reaction time of L-cys, $\text{K}_3[\text{Fe}(\text{CN})_6]$ and FeCl_3 (the formation time of L-cys-PBNPs/TBNPs), and reaction time between Cu^{2+} ion and L-cys-PBNPs/TBNPs were investigated and optimized for the detection of Cu^{2+} . In this study, the $\Delta\lambda$ was used to represent the sensitivity of the sensor for Cu^{2+} detection. The maximum absorption peak exhibited no obvious red shift after adding excessive Cu^{2+} . Therefore, the concentration of 2.5 μM of Cu^{2+} was chosen to study the sensitivity of the sensor and the high concentration of 100.0 μM of Cu^{2+} was set to study the degree of red shift ($\Delta\lambda_{\text{max}}$), which is related to the linearity range of the sensor.

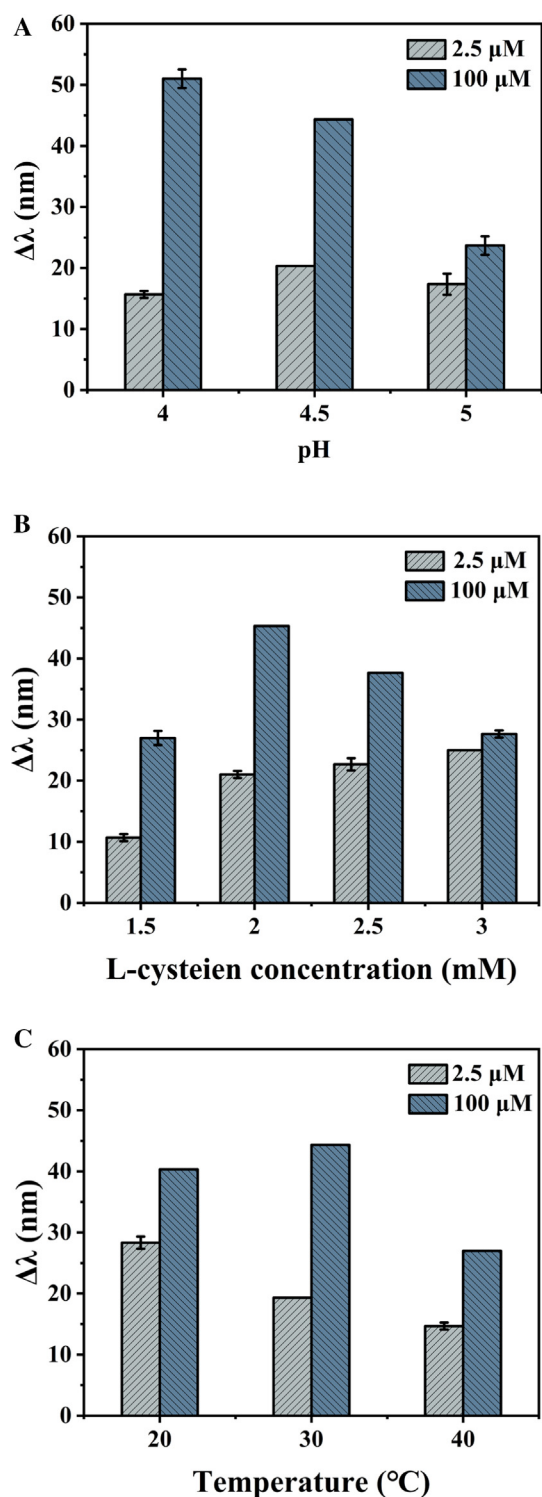


Fig. 4 Effects of NaAc-HAc buffer pH (A), L-cys concentration (B), and reaction temperature between L-cys-PBNPs/TBNPs and Cu^{2+} (C) on the determination of Cu^{2+} .

The effect of pH of NaAc-HAc buffer was investigated, and the result is shown in Fig. 4A. It is obvious that the $\Delta\lambda_{\text{max}}$ is decreased as the increase in the pH of NaAc-HAc buffer, but the $\Delta\lambda$ reaches a maximum at pH 4.5, indicating a better interaction between L-cys-PBNPs/TBNPs and Cu^{2+} . Hence,

considering a higher sensitivity of the sensor, pH 4.5 was selected as the optimal pH for the sensing system.

Furthermore, the effects of L-cys concentration on the $\Delta\lambda$ and $\Delta\lambda_{\max}$ were investigated, and the results are displayed in Fig. 4B. It can be observed that as the concentration of L-cys is increased up to 2.0 mM, the $\Delta\lambda$ remains nearly the same. The $\Delta\lambda_{\max}$ increases and reaches to a maximum at 2.0 mM and then decreases. Therefore, the optimal concentration of L-cys for the reaction was maintained at 2.0 mM. In addition, the reaction temperature between L-cys-PBNPs/TBNPs and Cu^{2+} was studied. Fig. 4C displays that as the temperature is increased from 20 to 40 °C, the $\Delta\lambda$ is decreased. Although the $\Delta\lambda_{\max}$ reaches a maximum at 30 °C, the $\Delta\lambda$ at 20 °C is much larger than that of at 30 °C. Therefore, considering a higher sensitivity of the sensor, 20 °C was chosen to be the optimal temperature in the following experiments.

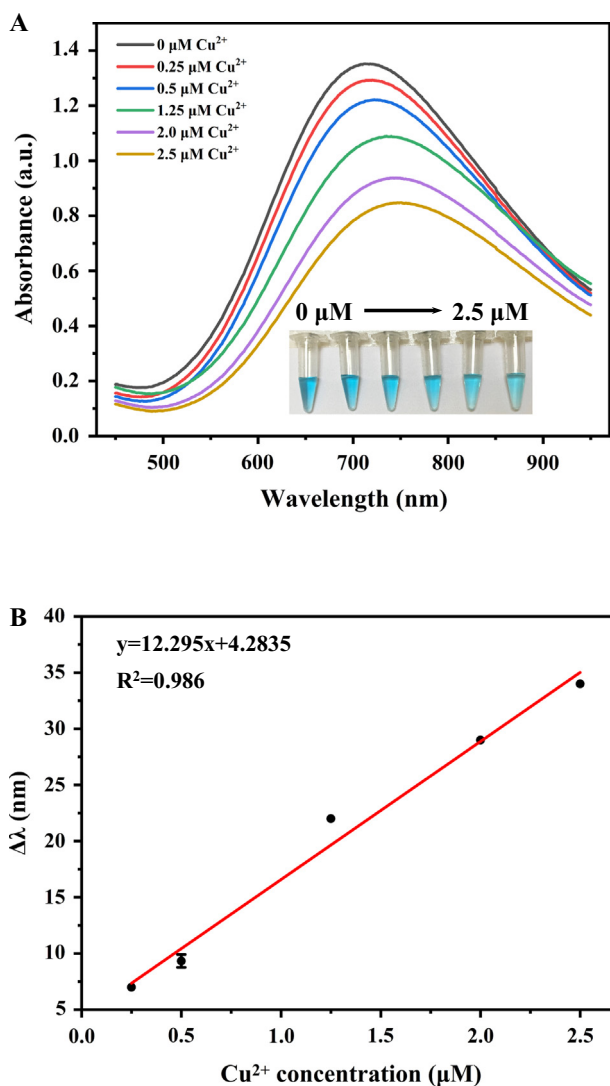


Fig. 5 UV-Vis spectra of the mixture containing Cu^{2+} at different concentrations and the inset image shows the corresponding solutions (A). Linear response between Cu^{2+} concentration and $\Delta\lambda$ (B). The error bar represents the standard deviations of three independent measurements.

Finally, the formation time of L-cys-PBNPs/TBNPs and reaction time between Cu^{2+} and L-cys-PBNPs/TBNPs were studied. As shown in Fig. S7A, 5.0 min is determined to be the optimal time of the formation of L-cys-PBNPs/TBNPs. It can be observed that both the $\Delta\lambda$ and $\Delta\lambda_{\max}$ remain the same after reacting for >2.0 min (Fig. S7B), indicating the completed reaction between L-cys-PBNPs/TBNPs and Cu^{2+} . Hence, 2.0 min was selected as the optimal reaction time between L-cys-PBNPs/TBNPs and Cu^{2+} . In summary, the optimal values for pH, L-cys concentration, reaction temperature between L-cys-PBNPs/TBNPs and Cu^{2+} , formation time of L-cys-PBNPs/TBNPs, and reaction time between L-cys-PBNPs/TBNPs and Cu^{2+} are pH 4.5, 2.0 mM, 5.0 min, and 2.0 min, respectively. The detection of Cu^{2+} can be completed rapidly in 7.0 min.

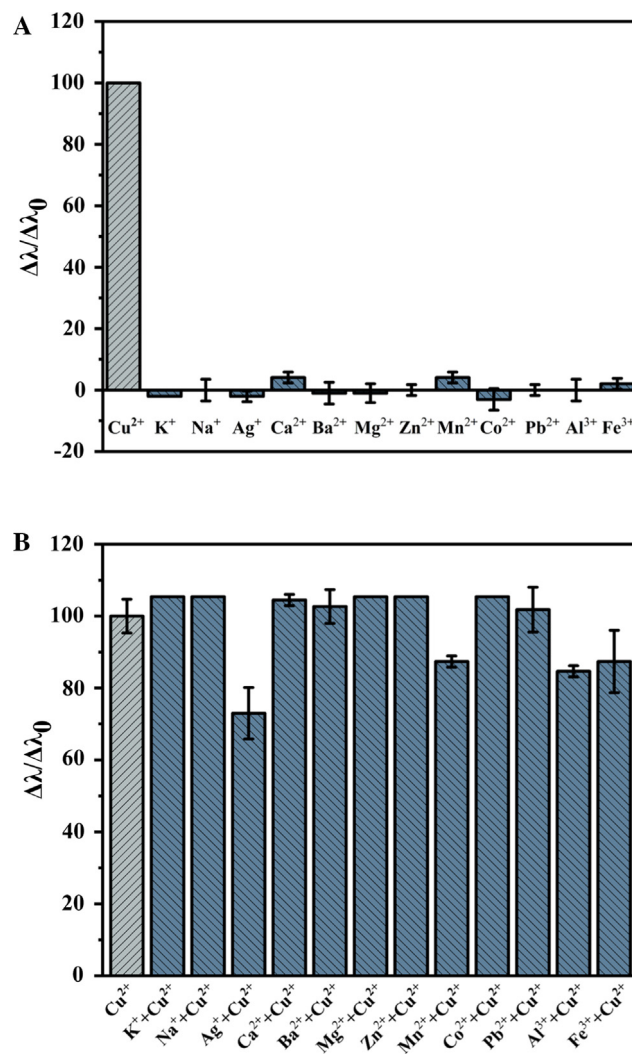


Fig. 6 The selectivity of the colorimetric sensor for Cu^{2+} detection over other metal ions (A). The interference evaluation of other metal ions towards this assay for Cu^{2+} (B). $\Delta\lambda/\Delta\lambda_0$ is the ratio (%) of peak shift value of adding interfering substance (A) or interfering substance + Cu^{2+} (B) to adding Cu^{2+} , which is set as 100%.

Table 1 Detection of Cu²⁺ in lake samples (*n* = 3).

Sample	Added (μM)	Found (μM)	Recovery (%) ^a	RSD (%) (<i>n</i> = 3)
Jin Lake	0	0 ^b	–	–
	0.500	0.519	103.8	7.4
	1.250	1.333	106.6	5.0
	2.500	2.417	96.7	1.6
Yun Lake	0	0	–	–
	0.500	0.519	103.8	7.4
	1.250	1.278	102.2	3.0
	2.500	2.498	99.9	1.5

^a Recovery = (found concentration – original concentration)/added concentration × 100%.

^b The detection value is lower than the quantification limit of this method.

3.5. Sensitivity for the detection of Cu²⁺

To investigate the ability of the developed sensor for quantitative analysis of Cu²⁺, various concentrations of Cu²⁺ (0.25, 0.5, 1.25, 2, and 2.5 μM) were added to the colorimetric system and analyzed under the optimal conditions. After the reaction, UV–Vis absorption spectra were obtained (Fig. 5A). The obvious red shift of the maximum absorption peak and the decrease of the absorption can be observed as the increase in concentration of Cu²⁺ in the test solution. Additionally, an evident color change from blue to light blue can be distinguished by naked eyes in the inset of Fig. 5A. Furthermore, Fig. 5B represents a graphical plot of the Δλ vs. Cu²⁺ concentration. A good increase in the linear plot is observed in the concentration range of 0.25–2.5 μM of Cu²⁺ and its linear correlation coefficient is about 0.986. The limit of detection (LOD = 3 σ/S, σ: standard deviation (*n* = 11), S: slope of standard curve) value for Cu²⁺ is calculated to be 0.12 μM. The value is much lower than the MCL for Cu²⁺ in drinking water, *i.e.*, 20.0 μM regulated by EPA (Gao et al., 2017).

3.6. Specificity of the colorimetric sensor for Cu²⁺ detection

To evaluate the selectivity and specificity of the proposed sensor for Cu²⁺ detection, other metal ions that may exist in the environment water, such as Na⁺, K⁺, Ag⁺, Pb²⁺, Ca²⁺, Mn²⁺, Co²⁺, Mg²⁺, Zn²⁺, Ba²⁺, Fe³⁺, and Al³⁺, were separately added into the same reaction solution and analyzed under the optimal conditions. The 2.5 μM of Cu²⁺ and 5.0 μM of other metal ions were used. As it can be observed

in Fig. 6A, all the tested metal ions produced negligible response to the L-cysteine-PBNPs/TBNPs colorimetric probe as compared with Cu²⁺, demonstrating the excellent selectivity of the proposed sensor for Cu²⁺. Further interference study was conducted on a series mixtures of Cu²⁺ (2.5 μM) and each individual interfering metal ion (5.0 μM). No significant difference in the response of the L-cys-PBNPs/TBNPs probe to Cu²⁺ in the absence and presence of the above interfering metal ions except for Ag⁺. Ag⁺ gave the negative effect on the response of Cu²⁺, probably because that PBNPs can be converted to colorless silver ferrocyanide ions in the presence of Ag (I) (Huang et al., 2017). These results indicate that the proposed sensor exhibited attractive selectivity and specificity towards Cu²⁺.

3.7. Determination of Cu²⁺ in real water

The practical applicability of the sensor was tested through determination of Cu²⁺ in lake water. Two water samples were obtained from Yun Lake and Jin Lake at Chongqing University. All the water samples were filtered for four times to remove impurities. There is no Cu²⁺ detected in real water samples without addition of Cu²⁺ as shown in Table 1. And the samples were spiked with three levels of Cu²⁺ (0.50, 1.25, and 2.50 μM) and analyzed by the developed method. As shown in Table 1, the average recoveries are in the range of 96.7–106.6%, with the relative standard deviations (RSDs) less than 7.4% (*n* = 3). These results demonstrate the potential application of this method for the detection of Cu²⁺ in real sample.

3.8. Comparisons of the method performance

The performance of the colorimetric method for the detection of Cu²⁺ was compared with some reported colorimetric and fluorescent methods (Table 2). The proposed sensor exhibits a narrower linear range as compared with other reported colorimetric methods for Cu²⁺ detection. However, these methods need to prepare complex materials, such as triangular gold nanoplates (Chang et al., 2017) and AuNPs (Wang et al., 2010, Mehta et al., 2013, Ye et al., 2015). There was study utilizing the peroxidase-like activity of PBNCs to detect Cu²⁺, however, the linear range is narrow and the sensitivity is low (Kavitha et al., 2021). The fluorescent method presents a wide linear range but with low sensitivity (Lin et al., 2021). Our newly designed sensor exhibits good sensitivity and high selectivity towards Cu²⁺. What's more, comparing with PBNPs, AuNPs need to prepare in advance and require a high

Table 2 Comparisons of the methods for the detection of Cu²⁺ in water samples.

Methods	Materials used	Preparation time	Detection time	Linear range	LOD	Ref.
Colorimetry	PBNPs ^a	5 min	2 min	0.25–2.50 μM	0.12 μM	This work
Colorimetry	Triangular gold nanoplates	> 10 min	20 min	1 μM – 1 mM	1 μM	Chang et al., 2017
Colorimetry	AuNPs	> 30 min	35 min	0.5–10 μM	0.5 μM	Ye et al., 2015
Colorimetry	AuNPs	> 15 min	70 min	0.625–15 μM	0.29 μM	Wang et al., 2010
Colorimetry	AuNPs	> 50 min	–	1–10 mM	14.9 μM	Mehta et al., 2013
Colorimetry	PBNCs ^b	18.5 h	15 min	6–9 μM	7 μM	Kavitha et al., 2021
Fluorescent	AuNPs	> 24 h	3 min	0–108 μM	5.8 μM	Lin et al., 2021

^a NPs: nanoparticles.

^b NCs: nanocubes.

temperature in the preparation process. Therefore, the simple preparation of L-cys-PBNPs/TBNPs, low-cost, and rapid detection are the additional advantages of this method.

4. Conclusions

In summary, this study developed a simple, sensitive, and selective colorimetric sensor for the detection of Cu^{2+} using L-cys-PBNPs/TBNPs as the probe for the first time. In the presence of L-cys, Cu^{2+} can rapidly induce the aggregation of L-cys-PBNPs/TBNPs, thereby resulting in the red shift of its maximum absorption peak. A good linearity was obtained between the $\Delta\lambda$ and the concentration of Cu^{2+} with a LOD of 0.12 μM . In addition, the sensor has excellent selectivity and very good spiked recovery for the detection of Cu^{2+} in lake water samples. In short, this work provides a low-cost method for rapid (about 7.0 min) and selective detection of Cu^{2+} , which has a good application prospect in environmental analysis.

CRedit authorship contribution statement

Hang-Yu Zhou: Conceptualization, Methodology, Investigation, Writing – original draft. **Hao Zhang:** Conceptualization, Methodology, Funding acquisition. **Li-Jing Peng:** Investigation. **Wei-Yi Zhang:** Investigation. **Tao Tian:** Investigation. **Feng-Qing Yang:** Supervision, Project administration, Funding acquisition.

Declaration of Competing Interest

The authors declare that they have no known competing financial interests or personal relationships that could have appeared to influence the work reported in this paper.

Acknowledgements

This work was supported by the National Key Research and Development Program of China (No. 2021YFC2103300), and Chongqing Medical and Pharmaceutical College, China (YGZ2021301).

Appendix A. Supplementary material

Supplementary data to this article can be found online at <https://doi.org/10.1016/j.arabjc.2022.104000>.

References

- Aksuner, N., Henden, E., Yilmaz, I., Cukurovali, A., 2009. A highly sensitive and selective fluorescent sensor for the determination of copper (II) based on a schiff base. *Dyes Pigm.* 83 (2), 211–217. <https://doi.org/10.1016/j.dyepig.2009.04.012>.
- Chang, C.C., Wang, G., Takarada, T., Maeda, M., 2017. Iodine-mediated etching of triangular gold nanoplates for colorimetric sensing of copper ion and aptasensing of chloramphenicol. *ACS Appl. Mater. Interfaces.* 9 (39), 34518–34525. <https://doi.org/10.1021/acsami.7b13841>.
- Falcone, E., Okafor, M., Vitale, N., Raibaut, L., Sour, A., Faller, P., 2021. Extracellular Cu^{2+} pools and their detection: From current knowledge to next-generation probes. *Coord. Chem. Rev.* 433, <https://doi.org/10.1016/j.ccr.2020.213727>.
- Fu, G.L., Sanjay, S.T., Dou, M.W., Li, X.J., 2016. Nanoparticle-mediated photothermal effect enables a new method for quantitative biochemical analysis using a thermometer. *Nanoscale* 8 (10), 5422–5427. <https://doi.org/10.1039/C5NR09051B>.
- Gao, Q., Ji, L., Wang, Q., Yin, K., Li, J., Chen, L., 2017. Colorimetric sensor for highly sensitive and selective detection of copper ion. *Anal. Methods* 9 (35), 5094–5100. <https://doi.org/10.1039/C7AY01335C>.
- Griffith, W.P., 1962. Cyanide complexes of the transition metals. *Quart. Rev. Chem. Soc.* 16 (2), 188–207. <https://doi.org/10.1039/QR9621600188>.
- Huang, W., Liang, Y., Deng, Y.Q., Cai, Y.H., He, Y., 2017. Prussian Blue nanoparticles as optical probes for visual and spectrophotometric determination of silver ions. *Microchim. Acta* 184 (8), 2959–2964. <https://doi.org/10.1007/s00604-017-2328-7>.
- Itaya, K., Ataka, T., Toshima, S., 1982. Spectroelectrochemistry and electrochemical preparation method of Prussian blue modified electrodes. *J. Am. Chem. Soc.* 104 (18), 4767–4772. <https://doi.org/10.1021/ja00382a006>.
- Jing, L.J., Liang, X.L., Deng, Z.J., Feng, S.S., Li, X.D., Huang, M.M., Li, C.H., Dai, Z.F., 2014. Prussian blue coated gold nanoparticles for simultaneous photoacoustic/CT bimodal imaging and photothermal ablation of cancer. *Biomaterials* 35 (22), 5814–5821. <https://doi.org/10.1016/j.biomaterials.2014.04.005>.
- Kavitha, S., Mary Jelastin Kala, S., Anand Babu Christus, A., Ravikumar, A., 2021. Colorimetric determination of cysteine and copper based on the peroxidase-like activity of Prussian blue nanocubes. *RSC Adv.* 11 (59), 37162–37170. <https://doi.org/10.1039/d1ra06838e>.
- Kim, Y.R., Kim, H.J., Kim, J.S., Kim, H., 2008. Rhodamine-based “turn-on” fluorescent chemodosimeter for Cu (II) on ultrathin platinum films as molecular switches. *Adv. Mater.* 20 (23), 4428–4432. <https://doi.org/10.1002/adma.200801001>.
- Li, L., Li, B.X., 2009. Sensitive and selective detection of cysteine using gold nanoparticles as colorimetric probes. *Analyst* 134 (7), 1361–1365. <https://doi.org/10.1039/b819842j>.
- Lin, S., Liu, S., Dai, G., Zhang, X., Xia, F., Dai, Y., 2021. A click-induced fluorescence-quenching sensor based on gold nanoparticles for detection of copper (II) ion and ascorbic acid. *Dyes Pigm.* 195, <https://doi.org/10.1016/j.dyepig.2021.109726>.
- Liu, J.M., Wang, H.F., Yan, X.P., 2011. A gold nanorod based colorimetric probe for the rapid and selective detection of Cu^{2+} ions. *Analyst* 136 (19), 3904–3910. <https://doi.org/10.1039/c1an15460e>.
- Liu, J.M., Jiao, L., Lin, L.P., Cui, M.L., Wang, X.X., Zhang, L.H., Zheng, Z.Y., Jiang, S.L., 2013. Non-aggregation based label free colorimetric sensor for the detection of Cu^{2+} based on catalyzing etching of gold nanorods by dissolve oxygen. *Talanta* 117, 425–430. <https://doi.org/10.1016/j.talanta.2013.09.004>.
- Ma, Y.R., Niu, H.Y., Zhang, X.L., Cai, Y.Q., 2011a. Colorimetric detection of copper ions in tap water during the synthesis of silver/dopamine nanoparticles. *Chem. Commun.* 47, 12643–12645. <https://doi.org/10.1039/c1cc15048k>.
- Ma, Y.R., Niu, H.Y., Zhang, X.L., Cai, Y.Q., 2011b. One-step synthesis of silver/dopamine nanoparticles and visual detection of melamine in raw milk. *Analyst* 136 (20), 4192–4196. <https://doi.org/10.1039/c1an15327g>.
- Mehta, V.N., Kumar, M.A., Kailasa, S.K., 2013. Colorimetric detection of copper in water samples using dopamine dithiocarbamate-functionalized Au nanoparticles. *Ind. Eng. Chem. Res.* 52 (12), 4414–4420. <https://doi.org/10.1021/ie302651f>.
- Neff, V.D., 1978. Electrochemical oxidation and reduction of thin films of Prussian blue. *J. Electrochem. Soc.* 125 (6), 886–887. <https://doi.org/10.1149/1.2131575>.
- Nóbrega, J.A., Lopes, G.S., 1996. Flow-injection spectrophotometric determination of ascorbic acid in pharmaceutical products with the Prussian Blue reaction. *Talanta* 43 (6), 971–976. [https://doi.org/10.1016/0039-9140\(95\)01830-1](https://doi.org/10.1016/0039-9140(95)01830-1).
- Zietza, B.P., Dieterb, H.H., Lakomek, M., Schneidera, H., Keßler-Gaedtke, B., Dunkelberg, H., 2003. Epidemiological investigation

- on chronic copper toxicity to children exposed via the public drinking water supply. *Sci. Total Environ.* 302 (1–3), 127–144. [https://doi.org/10.1016/S0048-9697\(02\)00399-6](https://doi.org/10.1016/S0048-9697(02)00399-6).
- Qin, Z., Li, Y., Gu, N., 2018. Progress in applications of Prussian blue nanoparticles in biomedicine. *Adv. Healthcare Mater.* 7 (20), 1800347. <https://doi.org/10.1002/adhm.201800347>.
- Ramdass, A., Sathish, V., Babu, E., Velayudham, M., Thanasekaran, P., Rajagopal, S., 2017. Recent developments on optical and electrochemical sensing of copper (II) ion based on transition metal complexes. *Coord. Chem. Rev.* 343, 278–307. <https://doi.org/10.1016/j.ccr.2017.06.002>.
- Reguera, E., Fernández-Bertrán, J., Balmaseda, J., 1999. The existence of ferrous ferricyanide. *Transit Metal Chem.* 24 (6), 648–654. <https://doi.org/10.1023/A:1006942415737>.
- Trumbore, C.N., Ehrlich, R.S., Myers, Y.N., 2001. Changes in DNA conformation induced by gamma irradiation in the presence of copper. *Radiat. Res.* 155 (3), 453–465. [https://doi.org/10.1667/0033-7587\(2001\)155\[0453:CIDCIB\]2.0.CO;2](https://doi.org/10.1667/0033-7587(2001)155[0453:CIDCIB]2.0.CO;2).
- Wang, J.M., Zhang, L., Yu, L., Jiao, Z.H., Xie, H.Q., Lou, X.W., Sun, X.W., 2014. A bi-functional device for self-powered electrochromic window and self-rechargeable transparent battery applications. *Nat. Commun.* 5 (1), 4921. <https://doi.org/10.1038/ncomms5921>.
- Wang, Y., Yang, F., Yang, X., 2010. Label-free colorimetric biosensing of copper (II) ions with unimolecular self-cleaving deoxyribozymes and unmodified gold nanoparticle probes. *Nanotechnology* 21, (20). <https://doi.org/10.1088/0957-4484/21/20/205502>.
- Wei, Y.Y., Zhang, Y.Z., Song, D., Li, J., Xu, Z.R., 2021. Alkaline phosphatase-regulated in situ formation of chromogenic probes for multicolor visual sensing of biomarkers. *Talanta* 228, <https://doi.org/10.1016/j.talanta.2021.122222>.
- Witting, P.K., Bowry, V.W., Stocker, R., 1995. Inverse deuterium kinetic isotope effect for peroxidation in human low-density lipoprotein (LDL): a simple test for tocopherol-mediated peroxidation of LDL lipids. *FEBS Lett.* 375 (1–2), 45–49. [https://doi.org/10.1016/0014-5793\(95\)01172-B](https://doi.org/10.1016/0014-5793(95)01172-B).
- Ye, Y.J., Lv, M.J., Zhang, X.Y., Zhang, Y.X., 2015. Colorimetric determination of copper (II) ions using gold nanoparticles as a probe. *RSC Adv.* 5 (124), 102311–102317. <https://doi.org/10.1039/c5ra20381c>.
- Yeon, S.Y., Seo, M., Kim, Y., Hong, H., Chung, T.D., 2022. Paper-based electrochromic glucose sensor with polyaniline on indium tin oxide nanoparticle layer as the optical readout. *Biosens. Bioelectron.* 203, <https://doi.org/10.1016/j.bios.2022.114002>.
- Yin, K., Li, B., Wang, X., Zhang, W., Chen, L., 2015. Ultrasensitive colorimetric detection of Cu²⁺ ion based on catalytic oxidation of L-cysteine. *Biosens. Bioelectron.* 64, 81–87. <https://doi.org/10.1016/j.bios.2014.08.058>.
- Zareba, J.K., Szeremeta, J., Waszkielewicz, M., Nyk, M., Samoć, M., 2016. Nonlinear-optical response of Prussian blue: Strong three-photon absorption in the IR region. *Inorg. Chem.* 55 (19), 9501–9504. <https://doi.org/10.1021/acs.inorgchem.6b01556>.
- Zargar, B., Hatamie, A., 2014. Prussian blue nanoparticles: a simple and fast optical sensor for colorimetric detection of hydralazine in pharmaceutical samples. *Anal. Methods* 6 (15), 5951–5956. <https://doi.org/10.1039/c4ay00618f>.
- Zhang, W., Hu, S.L., Yin, J.J., He, W.W., Lu, W., Ma, M., Gu, N., Zhang, Y., 2016. Prussian blue nanoparticles as multienzyme mimetics and reactive oxygen species scavengers. *J. Am. Chem. Soc.* 138 (18), 5860–5865. <https://doi.org/10.1021/jacs.5b12070>.
- Zhang, X., Rao, H., Huang, H., Zhang, K., Wei, M., Luo, M., Xue, X., Xue, Z., Lu, X., 2021. A sensitive photothermometric biosensor based on redox reaction-controlled nanoprobe conversion from Prussian blue to Prussian white. *Anal. Bioanal. Chem.* 413, 6627–6637. <https://doi.org/10.1007/s00216-021-03629-5>.